# Correlation between mechanical and structural properties as a function of temperature within the TeO2–TiO2–ZnO ternary system

J. de Clermont-Gallerande, Maggy Colas, F. Celarie, Y. Gueguen, M. Bergler, D. de Ligny, T. Hayakawa, P. Thomas

# Correlation between mechanical and structural properties as a function of temperature within the $TeO_2$-$TiO_2$-ZnO ternary system.

J. de Clermont-Gallerande[1] ; M. Dutreilh-Colas[1] ; F. Célarié[2] ; Y. Gueguen[2] ; M. Bergler[3] ; D. de Ligny[3] ; T. Hayakawa[4] ; P. Thomas[1]

[1]Institut de recherche sur les céramiques (IRCER), UMR 7315 CNRS / Université de Limoges, Centre Européen de la Céramique, 12, rue Atlantis, 87068 Limoges, France

[2] Institut de Physique de Rennes (IPR), UMR6251 CNRS, Universite de Rennes, 263 Avenue Général Leclerc, 35700 Rennes, France

[3] Institute of Glass and Ceramics, DMSE, University of Erlangen-Nuremberg, DE 91058 Erlangen, Germany

[4]Field of Advanced Ceramics, Department of Life Science and Applied Chemistry / Frontier Research Institute of Materials Science (FRIMS), Nagoya Institute of Technology, Gokiso, Showa, Nagoya 466-8555, Japan

## Abstract

In situ Raman spectroscopy, Resonance Frequency and Damping Analysis (RFDA) setup and Associated Raman Brillouin Calorimeter (ARABICA) setup experiments as a function of temperature were conducted on the (100-x)$TeO_2$-5$TiO_2$-xZnO (x=15; 17.5; 20; 22.5; 25) glass system. Structural and mechanical properties showed non-conventional properties evolution as a function of ZnO content which are managed by the modification of ZnO polyhedra. Before glass transition temperature (Tg), the evolution of the Boson peak (BP) frequencies and the elastic properties are in accordance with the idea of the relaxation of the strains inside the glass; after Tg, their evolution shows the transition toward a viscous liquid. BP and mechanical properties study evidences that as nano-heterogeneous domains size increases at a faster rate, the mechanical properties will decrease at a slower rate. This point will be helpful for choosing appropriate composition for optical fiber shaping.

## Introduction

Tellurite glasses have interested researchers in the field of photonic application for many years. Indeed, they are good candidates for optical fibers thanks to their high linear refractive index, high dielectric constant, wide infrared transmittance, and their high third order non-linear optical values (1–4).

Ab-initio studies showed that the pure $TeO_2$ glasses have the highest non-linear optical properties among tellurite glasses (5) (fifty times more than fused silica glasses (4,6)), but extreme quenching conditions are needed to obtain glass (7). Consequently, modifier oxides are required. Different systems have been studied in their abilities to form glasses (glassy domains) and their structural, linear and non-linear optical properties for many years in IRCER laboratory (8–14). Among them, adding $TiO_2$ is well known to increase the glass forming ability resulting in homogeneous glasses with only slight changes in the structure of pure $TeO_2$ glass (8,15,16).

Adding ZnO in tellurite glasses significantly increases the glass forming domain (up to 40mol% ZnO) (17). Binary $TeO_2$-ZnO glasses are useful media for ultra-low loss optical fibers (1 dB/km) in the wavelength range of 3.4-4 µm (18). Different studies have been done on $TeO_2$-ZnO glasses based on Raman spectroscopy data (19–23), and neutron and X-ray diffraction

(24). The different studies showed that adding ZnO to the original $TeO_2$ glass matrix results in *(i)* a structural transformation of $TeO_4$ into $TeO_3$ units and so a linear decrease of the optical properties *(ii)* a band gap decrease as the glasses turn more transparent upon adding ZnO (25).

The goal of the present study is to highlight a correlation between the evolution of the mechanical properties and the structure of (100-x)$TeO_2$-5$TiO_2$-xZnO (x=15, 17.5, 20, 22.5, 25 (TTZ) glasses as a function of temperature especially around the glass transition temperature (Tg). In this study, the medium-range structure of TTZ glasses is studied using in-situ Raman spectroscopy and mechanical properties by Resonance Frequency and Damping Analysis (RFDA) and Brillouin experiments (26). By looking at the properties of the glass as a function of temperature, it might be possible to have an idea of their ability to fiber shaping..

# 1. Experimental

## 1.1. Sample preparation

The relevant amount of the different initial powders (commercial: α-$TeO_2$: Toldini 99,9%, $TiO_2$: Aldrich 99%, ZnO : Alfa Aesar 99,99%) within the ternary system (100-x)$TeO_2$-5$TiO_2$-xZnO %mol, with x= 15; 17.5; 20; 22.5 and 25 (respectively named TTZ15, TTZ17.5, TTZ20, TTZ22.5 and TTZ25) were ground in a mortar then melted in a platinum crucible at 850°C before being quenched on a brass mold preheated at 150°C. The glass domain is smaller than the one found in (25) due to the amount of powder used (13g) to synthesize the samples for mechanical experiment. The obtained glasses were then annealed at 30°C below the glass transition temperature (taken from (25,27)) for 12 hours in order to release stresses resulting from the melt-quenching method. The final concentrations of the samples have been controlled by EDS experiments which evidence a deviation less than 2% from the theoretical composition.

As many experiments have been done, the size and synthesis conditions of the samples have been adapted to the needs of each measure. All the relevant information are summarized in the Table 1.

| Experiment | Initial mass (g) | Melting time (h) | Ground or polished | Form of the sample | Sample size (mm) |
|---|---|---|---|---|---|
| Raman spectroscopy | 2 | 1 | Ground | Powder | N/A |
| RFDA | 13 | 5 | Polished | Parallelepiped | l=30 |
| | | | | | L=15 |
| | | | | | e=3 |
| ARABICA* | 2 | 1 | Polished | Cylinder | D=3 |
| | | | | | h=1 |

*Table 1 : Information on the different experimental procedures for each experiment. *Associated Raman, Brillouin Calorimetry. D: diameter; h: height of a cylinder; l: length of a parallelepiped; L: width of a parallelepiped; e: thickness of a parallelepiped.*

Raman spectra were recorded in the 10-1000$cm^{-1}$ spectral range, using a T64000 HORIBA Jobin-Yvon spectrometer operating in the triple subtractive configuration at 514.5 nm. Samples were heat using a LINKAM TMS600 device (5°C/minute).

All Raman spectra were normalized (total area normalization) and baseline corrected (linear correction).

The normalized spectra were then decomposed using the Focus program (28) based on previous studies (10,25,29), with 10 oscillators: 9 Gaussian functions and 1 log-normal function. As the spectra are recorded at different temperature, all functions were independently

corrected from the Bose-Einstein factor. Due to the width and overlapping of the bands of the normalized Raman spectra (figure 1) all Gaussian functions were width at half maximum (FWHM) and frequency fixed, and only the intensity was left free. As the log-normal function is well defined, all fitting parameters were left totally free (frequency, FWHM and intensity).

The TTZ glass Raman spectra's frequencies range can be divided in two different parts: the low wavenumber region with the Boson peak (BP), the high wavenumber region (300-800 $cm^{-1}$) with the deformation of bridges (Zn-O-Zn or Zn-O-Te and asymmetric and symmetric Te-O-Te) and the elongation vibrations of Te-O bonds for $TeO_3$ and $TeO_4$ polyhedra (figure 2).

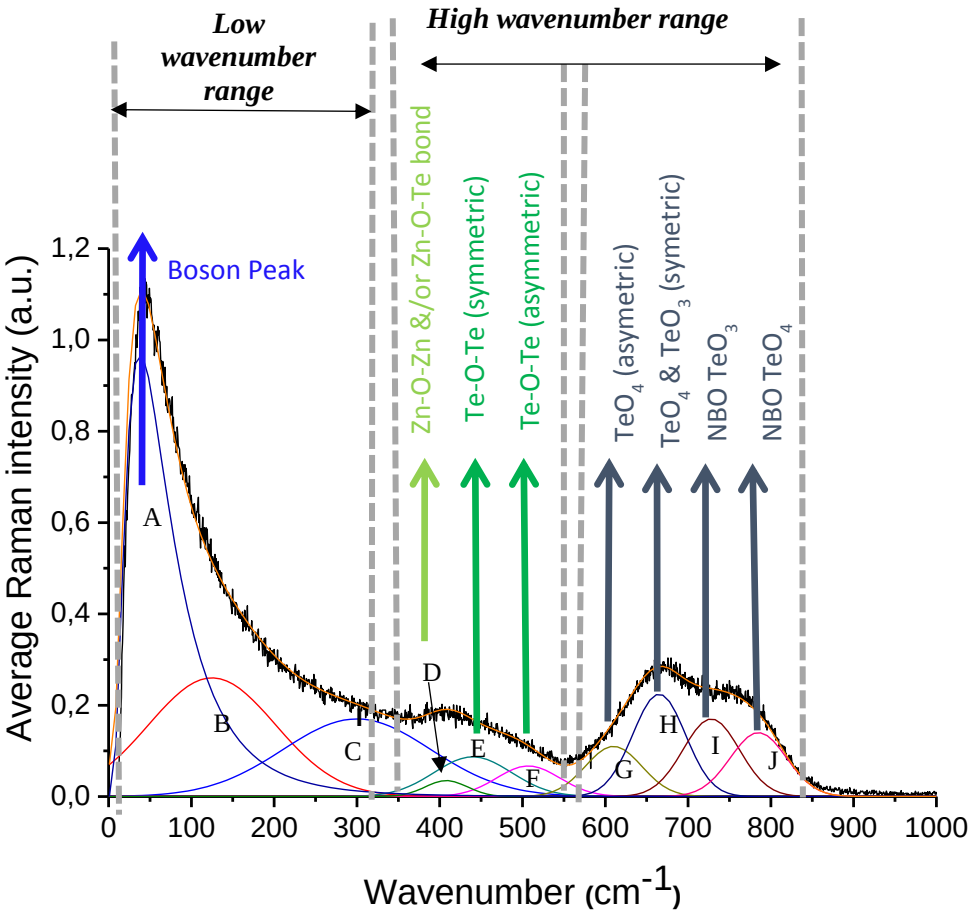


*Figure 1 : Raman bands attribution of a typical TTZ sample (Example of the TTZ15 sample)*

The mechanical properties have been obtained by Resonance Frequency and Damping Analysis (RFDA). Details on this technique can be found in the ASTM international base (26). Sample have been heat until the loss of the signal (10°C/minute).

Brillouin measurements have been done on the ARABICA platform (Associated Raman Brillouin Calorimetry) (30). Samples have been heated at 10°C/min until 420°C. Time accumulation from Brillouin signal is 30 seconds (spectrum each 5°C).

# 2. Results and discussion

## 2.1. Raman spectroscopy

Vibrational studies of $TeO_2$-ZnO glasses have been extensively done (19–21) at room temperature. It has been reported (20) that adding ZnO in the glasses has different

consequences. By Raman spectroscopy, a shift of the band corresponding to the vibration of the $TeO_4$ polyhedra toward higher frequencies and a shift of the band corresponding to the vibration of the non-bridging oxygen in $TeO_3$ and $TeO_4$ polyhedra to higher values accompanied by a progressive increase in intensity are observed. A decrease of the intensity of the band corresponding to the vibration of the Te-O-Te bridges and a shift to lower frequencies is also noted.

According to *Bürger et al*. (20), it has been evidenced that the introduction of zinc oxide in $TeO_2$ glasses will induce Non Bridging Oxygens (NBO) species. The length of one of the Te-O bond of the $TeO_4$ units gradually increase, leading into $TeO_{3+1}$ units and then $TeO_3$ units with an increase in zinc oxide content.

*Kozukharov et al*. reported that ZnO is introduced as $ZnO_6$ octahedra either within tellurite chains or between them (23). At low content of ZnO, a part of the $TeO_4$ trigonal bipyramids (tbps) becomes asymmetric, producing $TeO_{3+1}$ units observed in the $Zn_2Te_3O_8$ crystalline phase. For higher concentration of ZnO, the $TeO_{3+1}$ units loose one oxygen to become $TeO_3$ trigonal pyramids (tp) found in $ZnTeO_3$ crystalline phase (23).

*Thorbahn et al*. (24), evidenced by Raman spectroscopy and EXAFS experiments for binary $TeO_2$-ZnO glasses that Zn coordination number decreases from 6±1.6 to 4±0.6 with a Zn-O bond length that remained constant with increasing ZnO content. It was also reported that rather than the $ZnO_6$ configuration discussed above, ZnO is present in the form of $ZnO_4$ tetrahedra for high ZnO content (24).

In a previous study in IRCER laboratory, *Ghribi et al.* have studied the $TeO_2$-$TiO_2$-ZnO and the $TeO_2$-$GeO_2$-ZnO system at room temperature (25,29). They concluded that adding ZnO in glassy matrix will in a first step lead to breaking Te-O-Te bridges, including network depolymerization, and in a second step, with more ZnO content, to the formation of Te-O-Zn and Zn-O-Zn bridges.

As the role of ZnO in still unclear, we proposed here a structural investigation of the ternary system TTZ on a wide ZnO range content (15-25 mol%) from RT up to crystallization temperature. However, the crystallization of the samples won't be discuss in this paper.

Nevertheless, as parent crystallized phases give good indications of the unit, which can be evidence in glasses, an overview of crystallized phases in the $TeO_2$-ZnO binary system is proposed.

Two stable crystalline phases respectively $ZnTeO_3$ for 50% mol $TeO_2$ - 50% mol ZnO and $Zn_2Te_3O_8$ for 60% mol $TeO_2$ -40% mol ZnO (31,32) can be found (33).

The $Zn_2Te_3O_8$ structure is composed of chain-like structure with $Te_3O_8$ groups made with one $TeO_4$ and two $TeO_{3+1}$ units with $ZnO_{5+1}$ in octahedra-like structures between the chains.

Whereas, the $ZnTeO_3$ has Zn substituting Te to form new Zn-O-Te chains.

Pure ZnO crystal is made of chains of tetrahedra units.

By comparing each crystallized phases, it can be hypothesized that at low concentration of ZnO, the zinc polyhedra could be between the tellurite chains in a pseudo-octahedral form (looking like the $Zn_2Te_3O_8$ crystalline phase). And as ZnO content increases, the $TeO_4$ and $TeO_{3+1}$ polyhedra will decrease for an increase in $TeO_3$ polyhedra, the $ZnO_{5+1}$ polyhedra will also go toward a $ZnO_{4+1}$ and will substitute the tellurium oxide inside the chains to form Te-O-Zn bridges as shown in the $ZnTeO_3$ crystalline phase. It is possible that in glasses with high concentration in zinc oxide, the ZnO will be tetrahedra-formed inside the chains (as shown in the pure ZnO crystal). The crystallization of the samples have been presented elsewhere (33).

For an in-depth understanding of the vibration modes of the Raman spectroscopy of $Zn_2Te_3O_8$ and $ZnTeO_3$crystalline phases, computational studies by using LADY software (34) were done, and a theoretical Raman spectra was calculated for each phases.

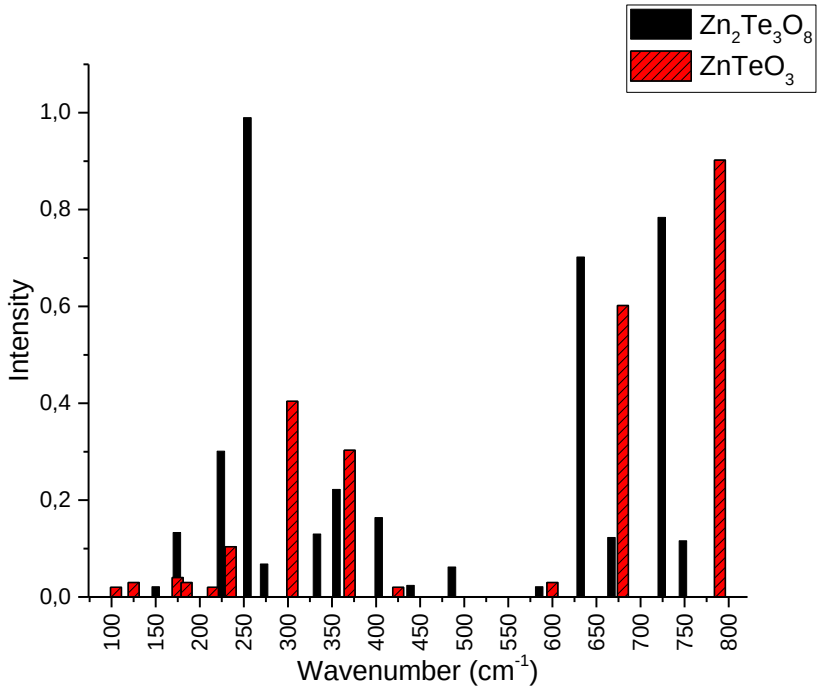


*Figure 2 : Simulated Raman spectra of the $Zn_2Te_3O_8$ and $ZnTeO_3$ crystalline phases*

By comparing the Raman spectra of the two crystalline phases (figure 2), the evolution of the Raman spectra as a function of the concentration can be explained. An increase of ZnO content causes : *(i)* an increase of the Zn-O-Zn/Zn-O-Te bonds (300-400 $cm^{-1}$), *(ii)* a decrease of the Te -O-Te bridges (400-550 $cm^{-1}$), *(iii)* a decrease of $TeO_4$ polyhedra and an increase of $TeO_3$ polyhedra (550-800 $cm^{-1}$) is expected.

As the Boson peak (BP) is a manifestation of the excess of Vibrationnal Density of States (VDoS), phonon scattering is caused by intrinsic density fluctuations domains in the structure (within which short and medium range order is maintained and beyond which the material is isotropic). The BP, which is characteristic of the glassy state, will give important information allowing the correlation of the mechanical and structural approaches. This paper will focus on its evolution.

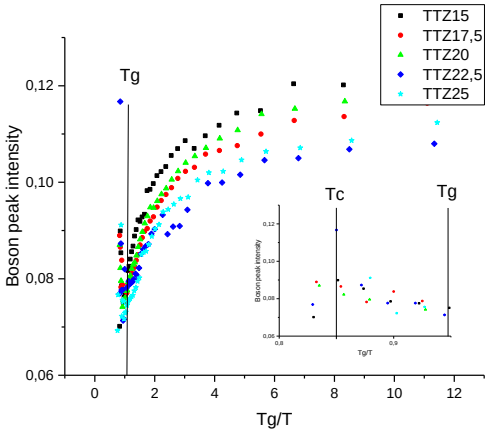


*Figure 3: BP intensity as a function of Tg/T. Inset: zoom of the variations around Tg*

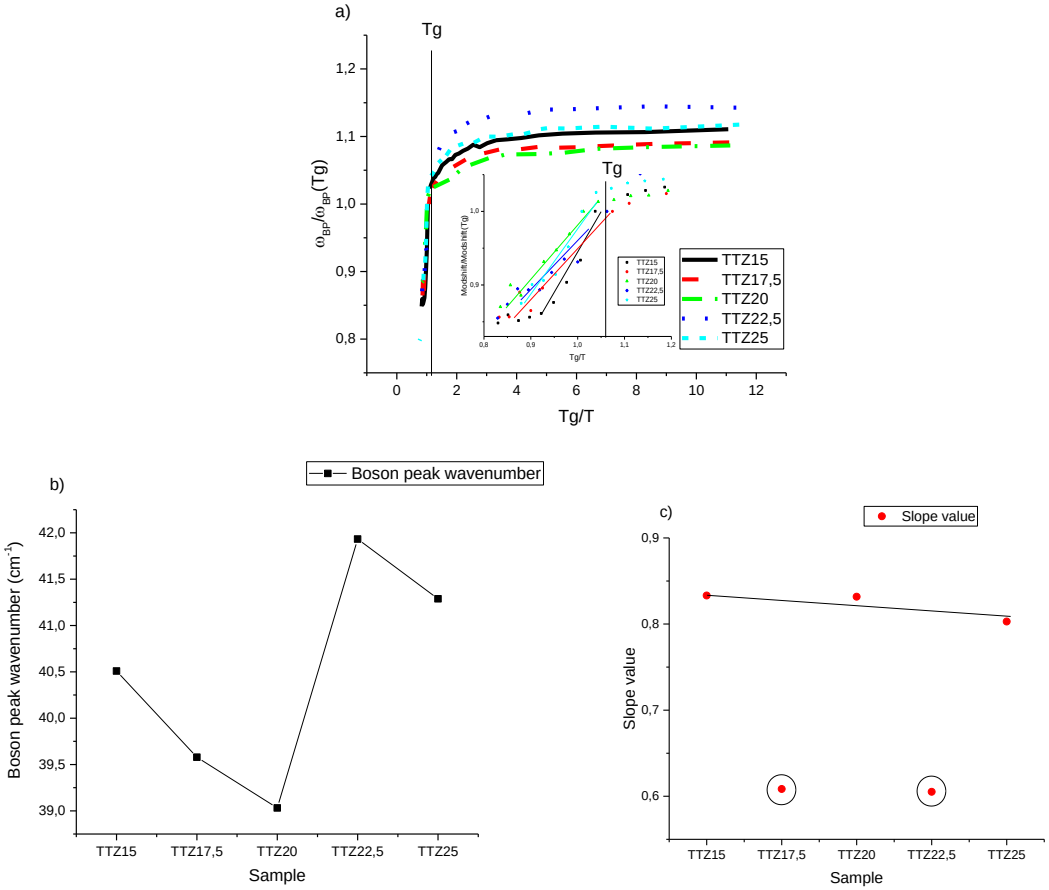


*Figure 4: **a)** $\omega_{BP}$ as a function of Tg/T. Inset: zoom of the variations around Tg **b)** $\omega_{BP}$ as a function of ZnO content at 30°C (RT). **c)** Average slope of data extracted from figure 4-a) after Tg*

Most of the graphs will be presented in a non-conventional way, namely abscissa and ordinate will be normalized by the value of the parameter under study at $Tg_{DSC}$ (obtained from DSC measurements,) to facilitate the comparison between samples.

Figure 3 represents the evolution of the Boson peak (BP) intensity. A decrease of the BP intensity before Tg is first observed and then followed by an increase up to crystallization temperature.

Figure 4a, b, c summarized the Boson peak wavenumber evolution. Figure 4a illustrates the general evolution of the Boson peak wavenumber of each sample as a function of temperature. A slight shift to lower wavenumber up to Tg, and after this temperature, a strong difference of the wavenumber evolution is observed. Figure 4b shows the Boson peak wavenumber as a function of the composition at Room temperature (RT). A decrease of the wavenumber with an increase of the ZnO concentration is observed until TTZ20 and a strong increase of this intensity is noted for further concentrations. To illustrate the evolution of the Boson peak wavenumber after Tg, Figure 4c represents the evolution of the slope of the curve shown in Figure 4a; this slope represents the rate at which the wavenumber of the Boson peak is decreasing after Tg. A slight decrease of the value between TTZ15, TTZ20 and TTZ25 can be noted and an abnormal behavior compared to the previous three samples was observed for TTZ17.5 and TTZ22.5 samples.

As a glass is considered composed of small domains with organized structure. Those domains (thereafter named blobs), are randomly arranged inside the glass, explaining its non-existent long order structuration.

When the BP intensity decreases, heterogeneity between blobs decreases (35,36). The present evolution means that with an increase in temperature, there is a rearrangement at short and intermediate distance of the glass to reach an energy minima at each temperature. After the glass transition temperature, the transition toward a viscous liquid will increase the heterogeneity of the glass. After the crystallization temperature, there is a decrease of intensity of the Boson peak due to the disappearance of the glass phase.

*Duval et al*. (37) and *Elliott et al*. (38) independently proposed a relationship between the size of the blobs $\xi$ ,the BP frequencies $\omega_{BP}$ and the mean sound velocities $V_{av}$ (see equation 3) calculated from the mechanical properties of the glasses. The evolution of $\omega_{BP}$ then gives a first understanding of the evolution of the size of the blobs as a function of the temperature.

$$\xi = V_{av}/\omega_{\mathrm{BP}} \quad (1)$$

In the present study, before Tg, a classical trend as a function of temperature is observed, as glass is relaxing the size of the blobs increases, and after Tg, the samples goes toward a state of a viscous liquid, increasing the size even further (figure 4a).

Figure 4b evidences that at RT, $\omega_{BP}$ decreases up to TTZ20 and then increases meaning that blobs size firstly increases and then decreases.

$\omega_{BP}$ fluctuations clearly evidences a change in the structural behavior of the glass.

## 2.2. Mechanical approach

### *2.2.1. RFDA*

The temperature dependence of the elastic moduli and the shear moduli are illustrated figure 8. As explained by *Mezeix et al*. (39) for silica glasses, a good description of the comportment of glasses at temperatures before Tg is obtained by using the model proposed by *Wachtman et al*. (40) (equation 2) and after Tg, this temperature dependence can be modeled by a power law equation proposed by *Rouxel et al*. (41) (equation 3).

$$G = G_{0K} - BT.\exp(\frac{-T_0}{T}) \quad (2)$$

$$G = G_{Tg}(\frac{Tg}{T})^{\alpha} \quad (3)$$

The obtained parameters of both simulated curves are reported on respectively table 2 (Wachtman parameters) and table 3 (Rouxel parameters). The intersection of both calculated curves gives the value Tg. As this temperature is dependent of the thermal history of the sample,

this temperature will be denoted mechanical Tg: $Tg_{RFDA}$. This $Tg_{RFDA}$ will be used to normalize the data.

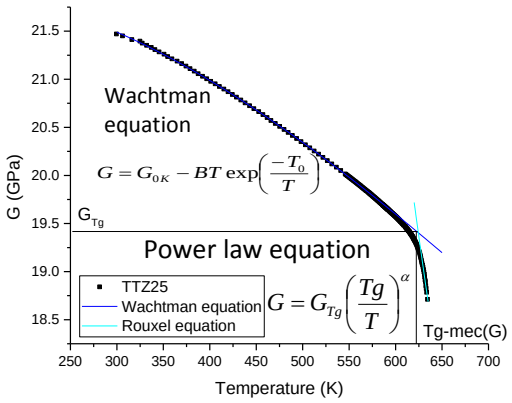


*Figure 5: Example of the shear modulus simulations as a function of temperature for the TTZ25 sample.*

| Sample | E | | | G | | |
|---|---|---|---|---|---|---|
| Wachtman parameters | $E_{0K}$ | **B** | $T_0$ | $G_{0K}$ | **B** | $T_0$ |
| TTZ15 | 52.45 | **0.023** | 531 | 21.30 | **0.011** | 588 |
| TTZ17.5 | 47.43 | **0.019** | 494 | 19.87 | **0.010** | 574 |
| TTZ20 | 51.34 | **0.018** | 353 | 20.87 | **0.009** | 503 |
| TTZ22.5 | 55.39 | **0.021** | 481 | 22.08 | **0.011** | 723 |
| TTZ25 | 54.25 | **0.029** | 700 | 21.89 | **0.011** | 634 |

*Table 2 : Wachtman equation simulation parameters for E and G curves*

| Sample | E | | | G | | |
|---|---|---|---|---|---|---|
| Rouxel parameters | $E_{Tg}$ | Tg(E) | **α** | $G_{Tg}$ | Tg(G) | **α** |
| TTZ15 | 48.38 | 593 | **1.26** | 30.06 | 383 | **1.01** |
| TTZ17.5 | 27.43 | 691 | **4.31** | 39.10 | 527 | **4.65** |
| TTZ20 | 30.33 | 722 | **2.79** | 24.20 | 514 | **1.45** |
| TTZ22.5 | 51.27 | 639 | **4.11** | 30.46 | 570 | **3.72** |
| TTZ25 | 29.82 | 717 | **3.66** | 26.09 | 547 | **2.25** |

*Table 3 : Rouxel equation simulation parameters for E and G curves*

The B parameter of the Watchman equation is quite constant for both E and G data, which means that the evolution of the properties are equivalent up to Tg. On the opposite, the evolution of the simulated alpha coefficient from the Rouxel equation evidences huge variations which means that after Tg, Young and shear modulus have special trend which has to be studied.

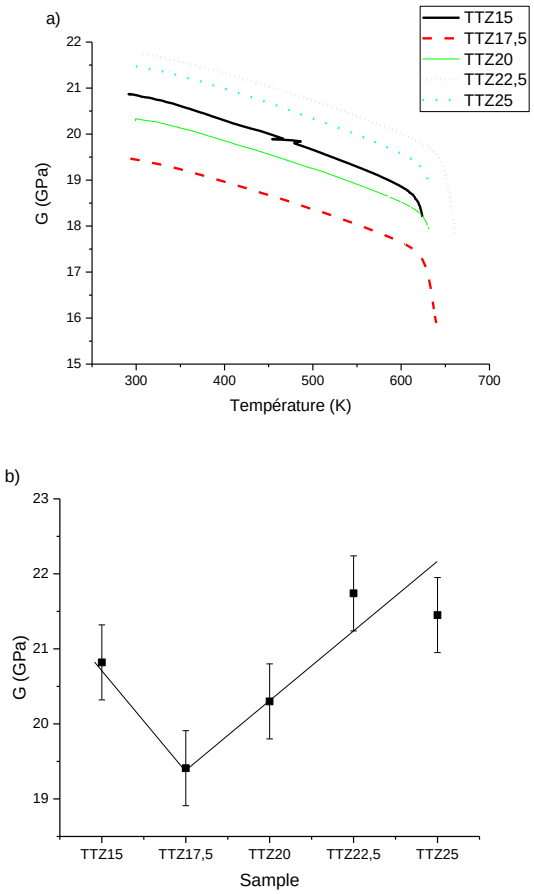


*Figure 6: **a)** Shear modulus as a function of temperature in the $TTZ_x$ (x=15; 17.5; 20; 22.5; 25) system. **b)** Shear modulus as a function of the concentration in ZnO at 30°C (RT)*

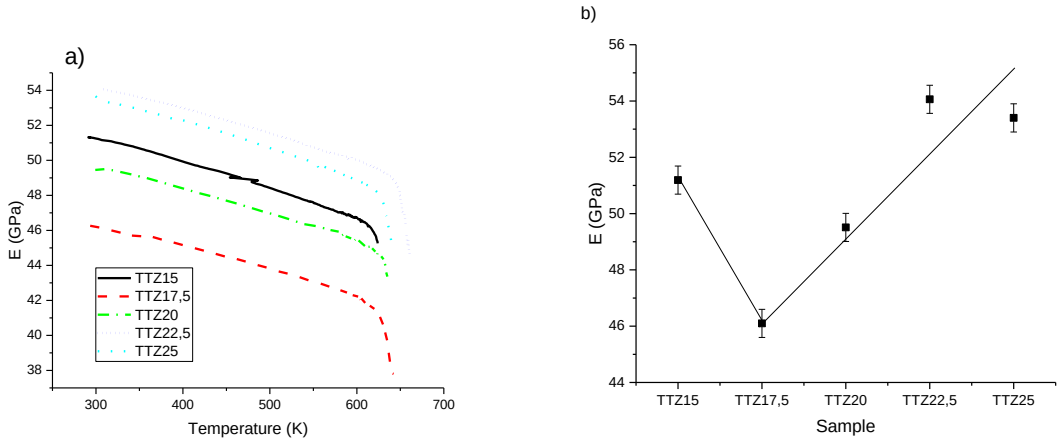


*Figure 7: **a)** Young modulus as a function of temperature in the $TTZ_x$ (x=15; 17.5; 20; 22.5; 25) system. **b)** Young modulus as a function of the concentration in ZnO at RT*

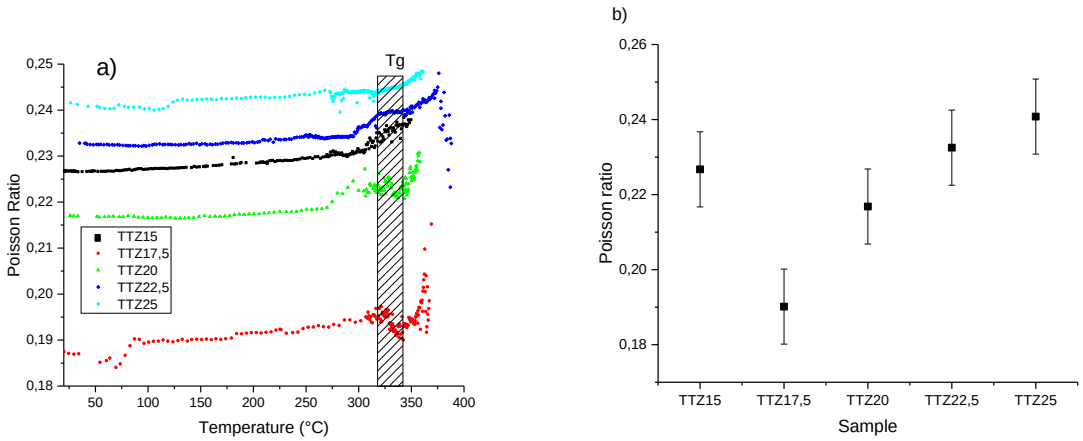


*Figure 8:* ***a)*** *Evolution of the Poisson ratio as a function of temperature,* ***b)*** *Evolution of the Poisson ratio as a function of the glass composition at RT*

As a function of temperature, for each sample, a slight decrease of E and G before $Tg_{RFDA}$ is observed which is exacerbated after (figure 6a and 7a). The Poisson ratio, which is calculated using G and E, presents also strong variations around Tg (figure 8a). This evolution will be further discussed in the discussion part.

The evolution of the E, G and ν values (figure 6b, 7b, 8b respectively) at room temperature and as a function of the concentration show an equivalent variation: a decrease of their values from TTZ15 to TTZ17.5 and then an increase from TTZ17.5 to TTZ25 is observed. Those results are consistent with the results previously published by *Ghribi et al.* (33), using ultrasonic echography experiments.

As Poisson ratio gives an information on the average connectivity of the glass (42), an increase of the connectivity of the network before TTZ17.5 and a decrease of the connectivity after is observed. Those results are consistent with the proposed theory: at low concentration of ZnO, Zinc oxide polyhedra are localized between the tellurite chains, linking them together by weak bonding, increasing by consequence the connectivity of the network but decreasing E and G values. At higher concentration, zinc atom substitutes Te atom within the chains, so it does not link the chains as it did at lower concentration. This in turn will decrease the connectivity of the network and increase once more E and G values compared to the lower concentration of zinc oxide.

The alpha coefficient (extracted from the Power law equation), which expresses the softening rate and which is correlated to the liquid fragility index (39), was calculated by measuring the slope of the curve obtained after plotting log(G/G(Tg)) versus f(log(Tg/T)) for temperatures higher than Tg (figure 9a). The same way is used for log (E/E(Tg))=f(log Tg/T)) (figure 9b).

The α coefficient evolution as a function of the concentration (figure 10) shows that the two glasses with the highest α value are the TTZ17.5 and TTZ22.5 samples. The other three glasses have a linear increase of the α coefficient value.

An higher value of α coefficient means a higher rate of decreasing mechanical properties, so the linear increase in the α coefficient value between TTZ15, TTZ20 and TTZ22.5 glasses means that the more ZnO content inside the glass, the faster the mechanical properties will decrease after Tg. The α coefficient for the two glasses TTZ17.5 and TTZ22.5 shows that the mechanical properties of these two glasses decrease at a faster rate.

Comparing the evolution of the TTZ17.5 glass to the previous conclusion on the structural properties, another hypothesis can be added: when the Zinc oxide is between the tellurite chains, the bonds between the Zinc oxide and the tellurium oxide are weak, and become even weaker after the glass transition temperature (decreasing at the same time the mechanical properties faster (higher α coefficient value)).

The evolution of the TTZ22.5 glass sample is still under study and other experiments are being done to understand the strange behavior of this sample compared to other compositions.

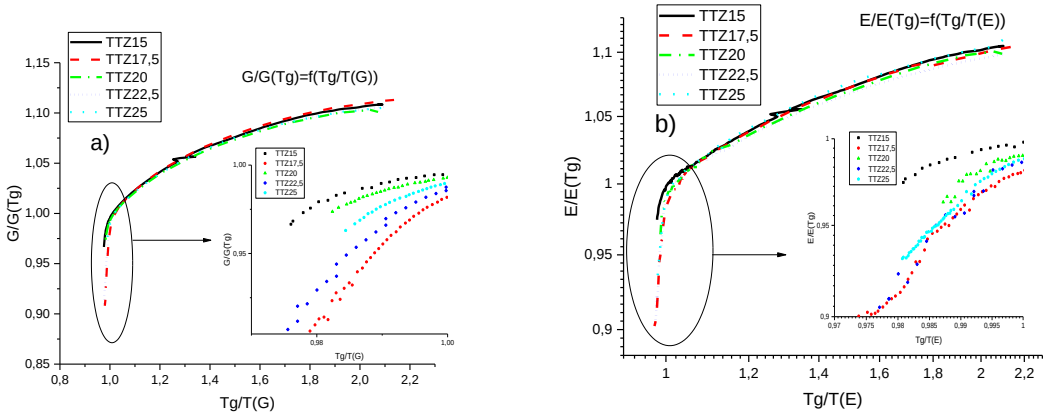


*Figure 9: **a)** G/G(Tg)=f(Tg/T); **b)** E/E(Tg)=f(Tg/T); Insets: zoom of the variations around Tg*

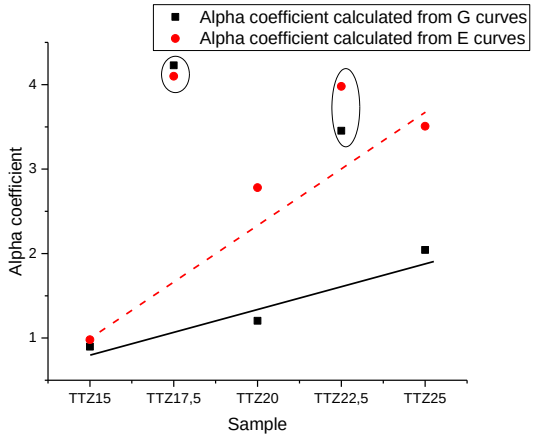


*Figure 10 : Alpha coefficient as a function of the ZnO concentration*

### *2.2.2. ARABICA experiment*

In the Brillouin spectra, due to the backscattering geometry used in the experimental setup only longitudinal mode are observed. The position of the Brillouin band strongly depends on the temperature (figure 11). A slight shift of the Brillouin position to lower energy before the glass transition temperature ($Tg_{DSC}$) is observed. Around 20°C before the glass transition temperature, a sharper decrease of the Brillouin shift is observed followed by a second slope break. The variation just before the glass transition temperature will be further discussed in the discussion part.

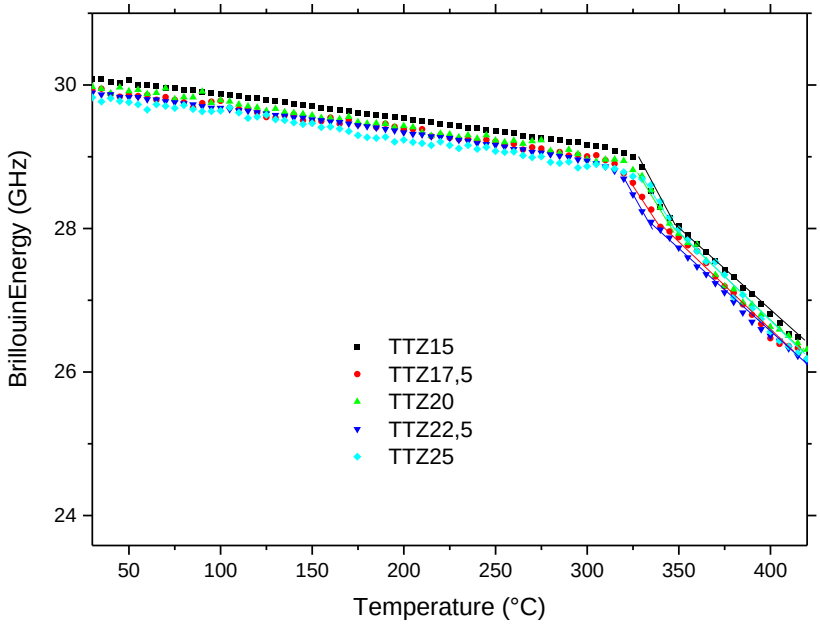


*Figure 11: TTZ glasses Brillouin position as a function of temperature*

As the Brillouin shift is proportional to the longitudinal velocity of the glasses, so proportional to the mechanical properties of each samples (equation 4). It is then possible to compare the mechanical properties obtained by RFDA experiments to the results from the Brillouin shift.

$$V_L(Brillouin) = \frac{\lambda.(Brillouin\ shift)}{2n} \quad (4)$$

With λ the wavelength of the measurement (488nm in this work) and n the linear refractive index at the same wavelength.

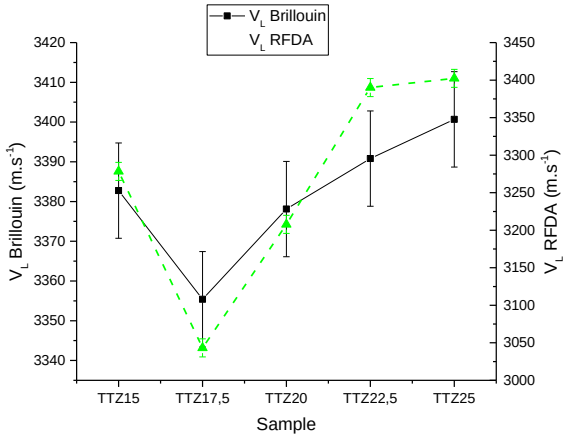


*Figure 12: Variation of the longitudinal velocities calculated from the Brillouin and RFDA experiments as a function of the concentration in zinc oxide at room temperature.*

Thanks to the figure 12, which compare the variation of the longitudinal velocities obtained by Brillouin experiment and RFDA experiment as a function of the ZnO content, a good agreement of the variation is found between the two different techniques, with a decrease of the longitudinal velocities between TTZ15 and TTZ17.5 followed by an increase thereafter.

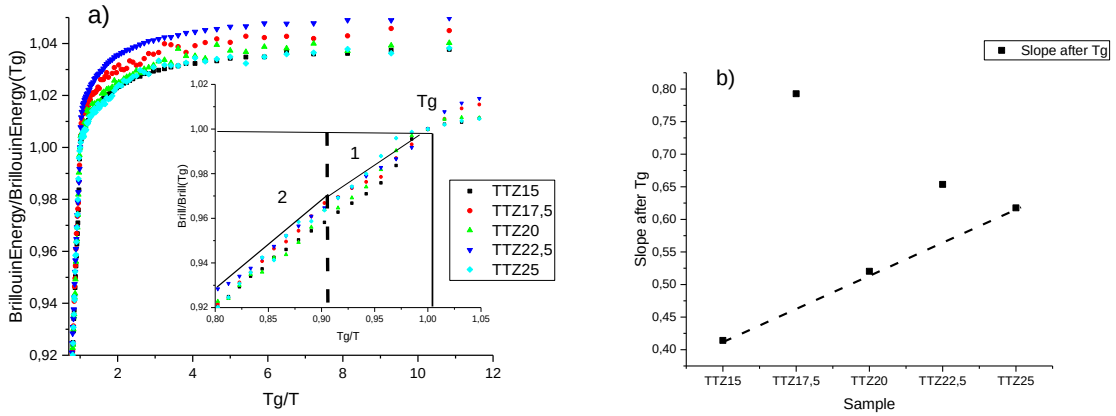


*Figure 13: **a)** Brillouin peak energy normalized with the Brillouin peak energy at the glass transition temperature as a function of Tg/T. Inset: zoom of the variations around Tg **b)** Variation of the slope in the second regime after the glass transition temperature*

By normalizing the Brillouin shift in the same way as for the mechanical properties to extract the alpha coefficient of the power law equation, it is possible to compare the evolution of the mechanical properties and the variation of the Brillouin energy by calculating the slopes in the second part of the graphic in figure 13a.

Hence, by comparing the values of slope calculated showed in figure 13b to the one from the α coefficient (figure 10), it is shown that the evolution as a function of the concentration has the same linear evolution between the three samples TTZ15, TTZ20 and TTZ25 with two anomalies being TTZ17.5 and TTZ22.5.

The results of the Brillouin experiment are in a good agreement with the mechanical properties as a function of the concentration but also as a function of temperature, with a slight decrease of the Brillouin shift as the mechanical properties decrease, and so even after Tg.

### 2.3. Discussion

| Sample | $Tg_{Raman}$ (°C) (±10°C) | $Tg_{RFDA}$ (°C) | | $Tg_{Brillouin}$ (°C) (±10°C) | $Tg_{DSC}$ (°C) (±5°C) |
|---|---|---|---|---|---|
| | | Tg(E) (±5°C) | Tg(G) (±5°C) | | |
| TTZ15 | 310 | 339 | 336 | 336 | 335 |
| TTZ17.5 | 313 | 353 | 354 | 339 | 337 |
| TTZ20 | 321 | 354 | 347 | 341 | 339 |
| TTZ22.5 | 324 | 372 | 372 | 340 | 341 |
| TTZ25 | 331 | 355 | 351 | 345 | 343 |

*Table 4 : Glass temperature measured by the different experiments (The values of $Tg_{DSC}$ shown in table 3 were measured thanks to the ARABICA setup at the same time as the Brillouin shift measures).*

A first interesting comment can be done on the difference between the values of Tg obtained as a function of the technique used. Using the same method as for RFDA data to extract a mechanical Tg, Raman data have been fitted with linear functions before and after the slope break observed on data, the value of Tg is extracted at the intersection of the two fitted parts. Comparing $Tg_{Raman}$ and $Tg_{RFDA}$ to $Tg_{DSC}$, it can be seen that $Tg_{Raman}$ is lower and $Tg_{RFDA}$ is higher. This difference partly come from the difference of sample's size, the difference of the heating rate (5°C/min for Raman spectroscopy and 10°C/min for the RFDA and ARABICA

measurements). Moreover Raman data are obtained in a semi-dynamic way (Stop of the heating ramp during acquisition time) and not a dynamic one like RFDA and ARABICA data recording.

Now, looking at Brillouin and RFDA experiments (in particular the Poisson coefficient) more in details, some interesting facts can be noted:

In Brillouin experiment (figure 11), Brillouin shift evolution exhibits an intermediate slope break between the glassy state and the liquid one: This intermediate domain is characteristic of relaxation events suggesting that the heating rate of 10°C/min used for the experiment was too fast, creating strains inside the glass. The intercept between the intermediate and the liquid part is equivalent to the $Tg_{DSC}$ and was used to define the $Tg_{Brillouin}$ (results shown on table 4).

By comparing the Brillouin data to the Raman data it can be noticed in Figure 14 that the $Tg_{Raman}$ corresponds to the intercept of the linear extrapolation between the glassy state and the liquid one of the Brillouin shift (relaxation temperature ($T_R$) values in table 5). This also corresponds to the strong variation around Tg found on the Poisson ratio curve (figure 9), where the variation in Poisson ratio starts to fluctuate (values in table 5). This means that the relaxation of the sample due to the high heating rate will strongly affect the connectivity of the network before the glass transition temperature, due to a rearrangement of the glassy network.

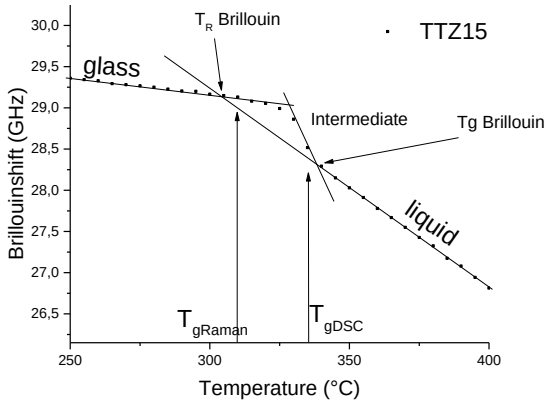


*Figure 14 : Example of how the relaxation temperature and the glass transition temperature are obtained (TTZ15 glass)*

| Sample | $T_R$ Brillouin (°C) | $T_R$ RFDA (°C) |
|---|---|---|
| TTZ15 | 303 | 305 |
| TTZ17.5 | 307 | 306 |
| TTZ20 | 312 | 309 |
| TTZ22.5 | 307 | 301 |
| TTZ25 | 322 | 316 |

*Table 5 : Relaxation temperatures for each samples in RFDA and Brillouin experiments*

To go further, as explained before, *Duval et al.* (37) and *Elliott et al.* (38) independently found a relationship that links the size of density fluctuations domains $\xi$ with the position of the Boson peak frequency $\omega_{BP}$ and the sound velocities inside the glasses.

$$\xi = \frac{V_{av}}{\omega_{BP}} \quad (3)$$

With $V_{av}$ the average between the transversal velocity ($V_T$) and the longitudinal velocity ($V_L$). It is possible to calculate the two required velocities with the two equation below

$$V_T = \sqrt{\frac{G}{\rho}} \qquad V_L = \sqrt{\frac{K + \frac{4G}{3}}{\rho}} \qquad K = \frac{1}{3}.\frac{E}{1-2\nu} \tag{4}$$

With K the Bulk modulus. $V_{av}$ is then calculated with the equation below.

$$V_{av} = \left(\frac{1}{3V_l^3} + \frac{2}{3V_t^3}\right)^{-1/3} \tag{5}$$

Figure 15a represents the evolution of the size of the domains as a function of temperature. Before the glass transition temperature, a slight increase of this parameter is evidenced, with a steeper increase after the glass transition temperature. This evolution is in accordance to the previous evolution of the Boson Peak, and correspond to the relaxation of the glass before Tg and then the transition toward a viscous liquid after Tg.

As a function of the concentration (Figure 15b), two different evolutions can be seen: a sharp decrease of the size of the blobs between TTZ15 and TTZ17.5 and hereafter data are almost constant. This means that drastic changes of the structure after TTZ17.5 are observed, which can be explained by the change of the Zn atom coordination number as a function of ZnO content.

The discrepancy between the evolution of the size of the blobs as a function of the concentration and the evolution of the Boson peak wavenumber comes from the evolution of the sound velocities, and by this bias the evolution of the mechanical properties. This also means that having the Boson peak wavenumber evolution isn't enough to understand exactly how the size of the blobs evolve, even if it can give a rough understanding of this evolution as shown as a function of temperature.

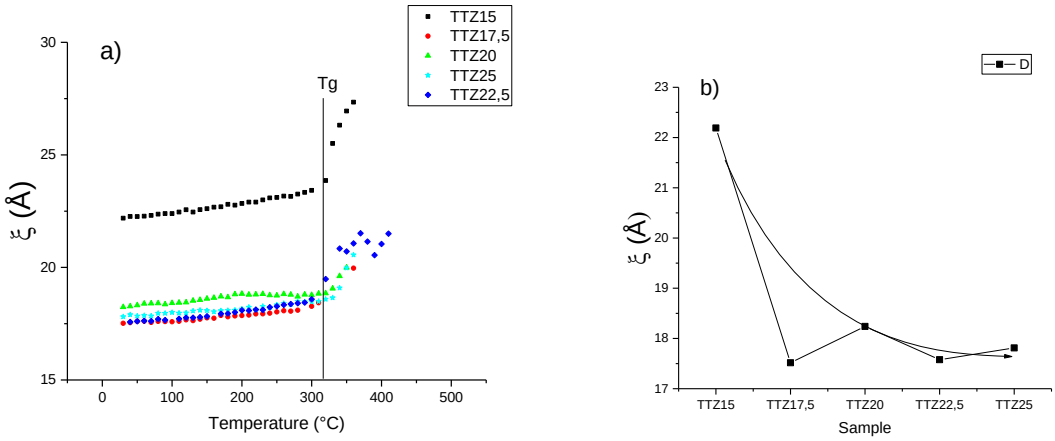


*Figure 15 : Evolution of the size of the blobs as a function of* ***a)*** *temperature;* ***b)*** *the concentration in ZnO (at RT)*

# 3. Conclusion

Correlation between structural properties of glasses to different kind of macroscopic physic one has been one of the most important field of research on glasses for years. In this study, some interesting facts have been pointed out.

By comparing RFDA experiments and Raman spectroscopy, it has been possible to understand the structural properties of a glass having a complex structure with two entities that have a coordination number which change as a function of the TeO2 and ZnO content. *(i)* As usual Raman spectroscopy gave informations on the change of the Te-O polyedra inside the

glass, *(ii)* RFDA experiment gave an understanding on the strength of the different bonds as a function of the concentration, and *(iii)* from both Raman and RFDA experiments by calculating the blobs size, the structural evolution of the glass at intermediate-distance has been evidenced.

Lastly, the behavior of the samples after the glass transition temperature has been evidenced and links to the particular behavior of Zinc polyhedra were noted. Indeed, the variation of the alpha coefficient of the mechanical properties studied by RFDA experiment, the variation of the slope after Tg of the Brillouin experiment and the variation of the slope of the shift in wavenumber of the Boson peak recorded in Raman spectroscopy, some anomalies stood out exactly at the same ZnO content : 17.5%ZnO and 22.5%ZnO.

Concerning mechanical properties, a higher slope value after the glass transition means that the decrease of the mechanical properties is faster

In Raman spectroscopy, a shift toward lower wavenumber means that the blobs size increases. So a higher slope value after the glass transition means that the blobs size increases at a higher rate.

From the two previous point, it can be porposed that: when the blobs size increase at a faster rate, the mechanical properties will decrease at a slower rate. Thanks to this hypothesis, it will be easier to predict how the mechanical properties will evolve at temperature close and higher than Tg which will be helpful for optical fiber shaping.

# 4. Acknowledgement

The authors thank Dr. J. Cornette for valued assistance with Raman experiments and O. Noguera for his help on Raman spectra simulation. J. de CLERMONT-GALLERANDE also gratefully acknowledges the financial support from Conseil Régional du Limousin and the PICS.

# Bibliography

[1] R. A. H. El-Mallawany, *Tellurite glasses handbook: physical properties and data*, 2nd ed. Boca Raton, FL: Taylor & Francis, 2011.

[2] A. P. Mirgorodsky, M. Soulis, P. Thomas, T. Merle-Méjean, and M. Smirnov, "*Ab initio* study of the nonlinear optical susceptibility of Te O 2 -based glasses," *Phys. Rev. B*, vol. 73, no. 13, Apr. 2006.

[3] J. S. Wang, E. M. Vogel, and E. Snitzer, "Tellurite glass: a new candidate for fiber devices," *Opt. Mater.*, vol. 3, no. 3, pp. 187–203, Aug. 1994.

[4] S.-H. Kim, T. Yoko, and S. Sakka, "Linear and Nonlinear Optical Properties of $TeO_2$ Glass," *J. Am. Ceram. Soc.*, vol. 76, no. 10, pp. 2486–2490, Oct. 1993.

[5] M. Soulis *et al.*, "Local molecular orbitals and hyper-susceptibility of $TeO_2$ glass," *J. Non-Cryst. Solids*, vol. 354, no. 2–9, pp. 199–202, Jan. 2008.

[6] J.-R. Duclère *et al.*, "Third order nonlinear optical properties of a paratellurite single crystal," *J. Appl. Phys.*, vol. 123, no. 18, p. 183105, May 2018.

[7] P. T. Sarjeant and R. Roy, "New Glassy and Polymorphic Oxide Phases Using Rapid Quenching Techniques," *J. Am. Ceram. Soc.*, vol. 50, no. 10, pp. 500–503, Oct. 1967.

[8] M. Udovic *et al.*, "Thermal characteristics, Raman spectra and structural properties of new tellurite glasses within the Bi2O3–TiO2–TeO2 system," *J. Solid State Chem.*, vol. 179, no. 10, pp. 3252–3259, Oct. 2006.

[9] M. Udovic *et al.*, "Formation domain and characterization of new glasses within the Tl2O–TiO2–TeO2 system," *Mater. Res. Bull.*, vol. 44, no. 2, pp. 248–253, Feb. 2009.

[10] D. Linda *et al.*, "New glasses within the Tl2O–Ag2O–TeO2 system: Thermal characteristics, Raman spectra and structural properties," *Mater. Res. Bull.*, vol. 45, no. 12, pp. 1816–1824, Dec. 2010.
[11] O. Noguera, T. Merle-Méjean, A. P. Mirgorodsky, P. Thomas, and J.-C. Champarnaud-Mesjard, "Dynamics and crystal chemistry of tellurites. II. Composition- and temperature-dependence of the Raman spectra of x(Tl2O)+(1−x) Te2O glasses: evidence for a phase separation?," *J. Phys. Chem. Solids*, vol. 65, no. 5, pp. 981–993, May 2004.
[12] M. Dutreilh-Colas, P. Charton, P. Thomas, P. Armand, P. Marchet, and J. C. Champarnaud-Mesjard, "The $TeO_2$-rich part of the $TeO_2$–$Ga_2O_3$ system: equilibrium and non-equilibrium phase diagram," *J Mater Chem*, vol. 12, no. 9, pp. 2803–2806, 2002.
[13] S. Blanchandin, P. Thomas, P. Marchet, J. C. Champarnaud-Mesjard, and B. Frit, "New heavy metal oxide glasses: investigations within the $TeO_2$–$Nb_2O_5$–$Bi_2O_3$ system," *J. Alloys Compd.*, vol. 347, no. 1–2, pp. 206–212, Dec. 2002.
[14] B. Jeansannetas *et al.*, "Glass Structure and Optical Nonlinearities in Thallium(I) Tellurium(IV) Oxide Glasses," *J. Solid State Chem.*, vol. 146, no. 2, pp. 329–335, Sep. 1999.
[15] M. Soulis, A. P. Mirgorodsky, T. Merle-Méjean, O. Masson, P. Thomas, and M. Udovic, "The role of modifier's cation valence in structural properties of $TeO_2$-based glasses," *J. Non-Cryst. Solids*, vol. 354, no. 2–9, pp. 143–149, Jan. 2008.
[16] M. R. Zaki, D. Hamani, M. Dutreilh-Colas, J.-R. Duclère, O. Masson, and P. Thomas, "Synthesis, thermal, structural and linear optical properties of new glasses within the $TeO_2$-$TiO_2$-$WO_3$ system," *J. Non-Cryst. Solids*, vol. 484, pp. 139–148, Mar. 2018.
[17] S. kareem Ahmmad, M. A. Samee, A. Edukondalu, and S. Rahman, "Physical and optical properties of zinc arsenic tellurite glasses," *Results Phys.*, vol. 2, pp. 175–181, 2012.
[18] L. G. Van Uitert and S. H. Wemple, "$ZnCl_2$ glass: A potential ultralow-loss optical fiber material," *Appl. Phys. Lett.*, vol. 33, no. 1, pp. 57–59, Jul. 1978.
[19] T. Sekiya, N. Mochida, and A. Ohtsuka, "Raman spectra of MO-$TeO_2$ (M = Mg, Sr, Ba and Zn) glasses," *J. Non-Cryst. Solids*, vol. 168, no. 1–2, pp. 106–114, Feb. 1994.
[20] H. Bürger, K. Kneipp, H. Hobert, W. Vogel, V. Kozhukharov, and S. Neov, "Glass formation, properties and structure of glasses in the $TeO_2$-ZnO system," *J. Non-Cryst. Solids*, vol. 151, no. 1–2, pp. 134–142, Dec. 1992.
[21] C. Duverger, M. Bouazaoui, and S. Turrell, "Raman spectroscopic investigations of the effect of the doping metal on the structure of binary tellurium-oxide glasses," *J. Non-Cryst. Solids*, vol. 220, no. 2–3, pp. 169–177, Nov. 1997.
[22] U. Hoppe, E. Yousef, C. Rüssel, J. Neuefeind, and A. C. Hannon, "Structure of zinc and niobium tellurite glasses by neutron and x-ray diffraction," *J. Phys. Condens. Matter*, vol. 16, no. 9, p. 1645, 2004.
[23] V. Kozhukharov, H. Bürger, S. Neov, and B. Sidzhimov, "Atomic arrangement of a zinc-tellurite glass," *Polyhedron*, vol. 5, no. 3, pp. 771–777, Jan. 1986.
[24] J. G. Thorbahn and J. W. Zwanziger, "Compositional dependence of the stress-optic response in zinc tellurite glasses," *J. Non-Cryst. Solids*, vol. 381, pp. 48–53, Dec. 2013.
[25] N. Ghribi *et al.*, "Thermal, optical and structural properties of glasses within the TeO2TiO2ZnO system," *J. Alloys Compd.*, vol. 622, pp. 333–340, Feb. 2015.
[26] ASTM International, "Standard Test Method for Dynamic Young's Modulus, Shear Modulus and Poisson's Ratio by Impulse Excitation of Vibration." ASTM E1876- 01, 2006.
[27] I. Kabalci, N. Ö. Körpe, T. Duran, and M. Özdemir, "Optical properties and crystallization kinetics of $(TeO_2)(ZnO)(TiO_2)$ glasses: Optical properties and crystallization kinetics of $(TeO_2)(ZnO)(TiO_2)$ glasses," *Phys. Status Solidi C*, vol. 8, no. 9, pp. 2629–2632, Sep. 2011.

[28] D. de Sousa Menses, *FOCUS version 1.0, software utility for the creation of optical function*. .
[29] N. Ghribi *et al.*, "Structural, mechanical and optical investigations in the TeO2-rich part of the $TeO_2$–$GeO_2$–ZnO ternary glass system," *Solid State Sci.*, vol. 40, pp. 20–30, Feb. 2015.
[30] A. Veber, M. R. Cicconi, H. Reinfelder, and D. de Ligny, "Combined Differential scanning calorimetry, Raman and Brillouin spectroscopies: A multiscale approach for materials investigation," *Anal. Chim. Acta*, vol. 998, pp. 37–44, Jan. 2018.
[31] K. Hanke, "Die Kristallstruktur von $Zn_2Te_3O_8$," *Naturwissenschaften*, vol. 53, no. 11, pp. 273–273, 1966.
[32] K. Hanke, "Zinktellurit: Kristallstruktur und Beziehungen zu einigen Seleniten," *Naturwissenschaften*, vol. 54, no. 8, pp. 199–199, 1967.
[33] N. Ghribi, *Synthesis, structural and mechanical investigations of new tellurite materials for non-linear optical applications*. Limoges, 2015.
[34] M. B. Smirnov and V. Y. Kazimirov, "LADY: Software for lattice dynamics simulations," *JINR Commun.*, vol. E14, p. 159, 2001.
[35] E. Duval *et al.*, "Inelastic light, neutron, and X-ray scattering related to the heterogeneous elasticity of glasses," *J. Non-Cryst. Solids*, vol. 307–310, pp. 103–108, Sep. 2002.
[36] B. Champagnon, L. Wondraczek, and T. Deschamps, "Boson peak, structural inhomogeneity, light scattering and transparency of silicate glasses," *J. Non-Cryst. Solids*, vol. 355, no. 10–12, pp. 712–714, May 2009.
[37] E. Duval, A. Boukenter, and T. Achibat, "Vibrational dynamics and the structure of glasses," *J. Phys. Condens. Matter*, vol. 2, no. 51, pp. 10227–10234, Dec. 1990.
[38] S. R. Elliott, "A Unified Model for the Low-Energy Vibrational Behaviour of Amorphous Solids," *Europhys. Lett. EPL*, vol. 19, no. 3, pp. 201–206, Jun. 1992.
[39] P. Mezeix, F. Célarié, P. Houizot, Y. Gueguen, F. Muñoz, and T. Rouxel, "Elasticity and viscosity of $BaO$-$TiO_2$-$SiO_2$ glasses in the 0.9 to 1.2Tg temperature interval," *J. Non-Cryst. Solids*, vol. 445–446, pp. 45–52, Aug. 2016.
[40] J. B. Wachtman, W. E. Tefft, D. G. Lam, and C. S. Apstein, "Exponential Temperature Dependence of Young's Modulus for Several Oxides," *Phys. Rev.*, vol. 122, no. 6, pp. 1754–1759, Jun. 1961.
[41] T. Rouxel, "Elastic Properties and Short-to Medium-Range Order in Glasses," *J. Am. Ceram. Soc.*, vol. 90, no. 10, pp. 3019–3039, Oct. 2007.
[42] G. N. Greaves, A. L. Greer, R. S. Lakes, and T. Rouxel, "Poisson's ratio and modern materials," *Nat. Mater.*, vol. 10, no. 11, pp. 823–837, Nov. 2011.